Journal homepage:http://revues.imist.ma/?journal=jasi

ISSN: 2550-4800

https://doi.org/10.48442/IMIST.PRSM/jasi-v10i1-3.27280

Superhydrophobic siloxane functionalized zirconia, stannia and ceria nanoparticles synthesized through a phyto-mediated route

F.O. Oyedeji [1], O.S . Bankole-Ojo [2,], N. Ramanuj [3]*

[1]*Department of Chemistry, University of Ibadan , Ibadan, Oyo State, Nigeria.*
[2]*Department of Physical Science, Crawford University, Faith city, Igbesa, Ogun State, Nigeria.*
[3]*Polymers and Functional Materials Division, Indian Institute of Chemical Technology, Hyderabad, Telangana State, India.*

Received 15 July 2021; Revised 13 September 2021; Accepted 19 September 2021.

Abstract: *The suitability of phyto-synthesized metal oxide nanoparticles for producing super-hydrophobic coatings for potential biomedical, agricultural and industrial applications was studied for the first time. ZrO_2, CeO_2 and SnO_2 nanoparticles were synthesized through a green and facile method by using the aqueous leaf extract of the widely distributed Azadirachta indica as capping agent with over 60 % percentage mass yield. Organic groups acting as capping/stabilizing agents and siloxane attachments were identified using Fourier transform infra-red (FTIR). Tiny spherical ZrO_2 nanoparticles, angular shaped CeO_2 particles and a bed of tiny SnO_2 particles with overall predominant particle sizes less than 15 nm were observed using field emission scanning electron microscope (FESEM). As expected, non-wettability of surfaces generally increased with increasing siloxane coupling of the nanoparticles. At a nanoparticle to fluoroalkylsilane mole ratio of 1:1, non-wettable, highly non-wettable and super-hydrophobic surfaces were obtained for CeO_2, SnO_2 and ZrO_2 nanoparticles, respectively. The extent of initial phytochemical adsorption, size of the nanoparticles and extent of agglomeration are major factors that influence the coupling of fluoroalkylsilanes and consequently, the wettability of surfaces produced.*

Keywords: *ZrO_2, CeO_2, SnO_2, Phyto-synthesis, Siloxane coupling, Super-hydrophobic surface.*

1. Introduction

Metal oxide nanoparticles for hydrophobic applications have been synthesized by physical and chemical methods such as sono-chemical [1], mechano-chemical [2], hydrothermal [3], microwave [4], co-precipitation [5], sol-gel [6] and several other techniques. However, most of the techniques are complex, time consuming, expensive and require the use of toxic solvents [7]. The green chemistry approach to the synthesis of metal oxide nanoparticles includes the use of plants for nanoparticle synthesis. This method offers plenty of advantages such as low-energy consumption, cost-effectiveness, absence of toxic solvents and ease of up-scalabilty [8]. To the best of our knowledge, surface wettability properties of phytosynthesized metal oxide nanoparticles have not been studied. This study involves the use of three metal oxides that are often used in hydrophobic surface coatings, namely: ZrO_2, SnO_2 and CeO_2 nanoparticles. ZrO_2 nanoparticles are thermally and chemically stable nanoparticles with abundant oxygen vacancies, fracture toughness, wear resistance and hardness. CeO_2 nanoparticles have been studied to possess a high degree of surface defects and exhibit a superior ability in the storage of oxygen and diffusion oxygen vacancy at high temperatures.

It has been also gained that CeO_2 and SnO_2 nanoparticles have garnered tremendous interest in recent years due to their importance in the coatings industry. Several plants have been employed in the biological synthesis of ZrO_2 nanoparticles. Gowri et al. [9] used the aqueous extract of Aloe Vera. Nimare and Koser [10] used ethanolic leaf extracts of *Azadirachta indica* to synthesize ZrO_2 nanoparticles with zirconyl chloride octahydrate ($ZrOCl_2.8H_2O$) as the precursor. The aqueous extract of *Allium cepa* leaves, *Capsicum annum* fruits and *Lycopersicon* esculentum fruits were used by Jalill et al. [11] to obtain ZrO_2 nanoparticles. CeO_2 nanoparticles have also been synthesized using phytochemicals. Kannan and Sundrarajan [12] used aqueous extract of *Acalypha indica* to synthesize CeO_2 nanoparticles with sizes ranging from 8 nm to 54 nm with appreciable agglomeration. *Aloe barbadensis* miller gel was used by Priya et al. [13] to produce spherical CeO_2 nanoparticles with a mean diameter of 63.6 nm. Arumugam et al. [14] utilized aqueous leaf extract of *Gloriosa superba* to synthesize CeO_2 nanoparticles with an average particle size of 5 nm for its antibacterial properties. Thovhogi et al. [15] used the aqueous extract of *Hibiscus sabdariffa* flower to synthesize CeO_2 nanoparticles with an average particle size of 3.9 nm. Leaves of *Olea europaea* were recently used to synthesize spherical CeO_2 nanoparticles with an average size of 24 nm [16].

Few studies have been done on the synthesis of SnO_2 nanoparticles via the biological method. The bacterium *Erwinia herbicola* was used by Srivastava & Mukhopadhyay [17] to synthesize spherical SnO_2 nanoparticles with sizes ranging from 10 to 42 nm.

* *Corresponding author: E-mail: sciforch@hotmail.com (O.S. Bankole-Ojo)*

Kamaraj et al. [18] synthesized silver doped tin (IV) oxide nanoparticles using the methanolic extract of *Cleistanthus collinus* plant leaves. SnO_2 nanoparticles with a crystallite size of 49.26 nm were prepared using *Cleistanthus collinus* methanolic leaf extract. *Saraca indica* flower was utilized by Vidhu and Philip [19] to synthesize SnO_2 nanoparticles with sizes ranging from 2 to 4 nm. *Plectranthus amboinicus* leaf extract was used to synthesize SnO_2 nanoparticles with an average size of 63 nm for dye degradation [20].

Phytochemicals from the aqueous leaf extract of the widely distributed tropical plant *Azadirachta indica* were used in this study as capping and stabilizing agents for the synthesis of CeO_2 and SnO_2 nanoparticles. The aqueous leaf extract of *Azadirachta indica* has been proven to exhibit high anti-oxidant activity due to phytochemicals such as alkaloids, carbohydrates, reducing sugars, flavonoids, glycoside, tannins and saponins [21].

The recent surge of interest in the field of liquid-repellent surfaces as a result of their increasing application in anti-fouling, anti-friction and anti-corrosion coatings has led to many studies that highlight the contributions of the nanoparticle geometry, surface energy and chemical composition to surface wettability. Major synthetic methodologies used in the production of non-wettable surfaces include electro-spinning, particle impregnation, spraying, etching and lithography. [22] However, a greener and more affordable method achieved by the use of bio-synthesized nanoparticles remains an attractive route to the production of surfaces with considerable resistance to wetting.

The present paper describes the modification of phyto-synthesized ZrO_2, CeO_2 and SnO_2 nanoparticles via substitution of surface phytochemicals with siloxanes for the first time. It assesses the suitability of phyto-synthesized nanoparticles for the production of non-wettable surfaces. The nanoparticle to fluoroalkylsilane mole ratio was varied to study its impact on static contact angles. Studies were also conducted to assess the effect of reaction pH and calcination temperature on size and crystalline nature of the nanoparticles respectively.

2. Experimental

2.1. Plant Identification and collection

The *Azadirachta indica* leaves were collected between September and March from the botanical garden of CSIR-IICT, Tarnaka, Hyderabad, India (17º25'28.9"N, 78º.32'17.8"E) between 12 noon and 4 pm. Taxonomic identification was done by Dr. G. Baskar Rajan, the head of the botanical garden. The leaves were harvested by the gardeners.

2.2. Preparation of plant materials

The leaves of *Azadirachta indica* were washed with double distilled water and air dried for four days. The leaves were pulverized using a dedicated domestic blender and stored at 4 ºC in an air-tight, sterilized and dry glass container for further use.

2.3. Preparation of aqueous plant extract

10 g of finely pulverized leaves was added to 100 mL of double distilled water. It was heated at 100 ºC for 30 minutes under reflux with vigorous stirring and thereafter, allowed to cool. The aqueous extract was obtained after filtration. The filtrate was centrifuged at 10,000 rpm at 15 ºC for 10 minutes to remove the heavy biomolecules and prevent them from precipitating with nanoparticles during the purification process. The supernatant was obtained after decantation and filtered to separate any remaining particle. The aqueous extract was stored at 4 ºC for further use.

2.4. Synthesis of nanoparticles

Zirconium (IV) propoxide solution, 70 wt. % in 1-propanol, cerium (III) nitrate hexahydrate ($CeNO_3.6H_2O$) and tin (II) chloride dihydrate were used as precursors for synthesizing ZrO_2, CeO_2 and SnO_2 nanoparticles, respectively. The nanoparticles were synthesized according to the method used by Madhusudhana et al. [23] for ZrO_2, Priya et al. [13] and Arumugam et al. [14] for CeO_2 and by Fu et al. [20] for SnO_2 with some modifications.

The zirconium (IV) propoxide solution, 70 wt. % in 1-propanol was diluted to obtain a concentration of 1 mM. The precursor solution was hydrolyzed by adding the aqueous extract in a dropwise manner. For the synthesis of CeO_2 and SnO_2 nanoparticles, aqueous extract was added drop-wise to the 1 mM precursor solution.

For all the nanoparticles, a precursor solution to extract volume ratio of 4:1 was maintained for 30 minutes under continuous stirring at an ambient temperature of 35-40 ºC. 0.1 M solution of NaOH and H_2SO_4 were used to adjust the pH value.

2.5. Separation and purification of nanoparticles

The nanoparticles were precipitated out of solution via centrifugation at 10,000 rpm at 15 ºC for 10 minutes and re-dispersed in absolute ethanol while being sonicated using a bath sonicator for 10 minutes. The centrifugation-dispersion cycle was carried out three times to remove organic groups loosely adsorbed to the nanoparticle surface. The ethanolic suspension was evaporated at 60 ºC in a vacuum oven for 6 hours.

2.6. Calcination of nanoparticles

The dried nanoparticles were grinded and transferred into a crucible for calcination. Calcination was done at 600 ºC for 4 hours at a heating rate of 10 ºC per minute. As-synthesized and calcined nanoparticles were kept at 4 ºC in 1.5 mL Eppendorf tubes for further characterization.

2.7. Functionalization of nanoparticles

Tridecafluorooctyltriethoxysilane (FAS 8261), a bifunctional fluoro-alkylsilane that possesses hydrolysable ethoxysilyl groups and a fluoroalkyl chain was used as the surface coupling agent to produce siloxane functionalized nanoparticles. Functionalization was carried out by using Pazokifard et al. [24] method with slight modifications.

Nanoparticles were dispersed in 30 mL anhydrous ethanol under the influence of a bath sonication for 10 minutes. A measured volume of FAS 8261 was gradually added to the nanoparticles in ethanol using a hypodermic syringe to achieve nanoparticle: fluoroalkylsilane: ethanol mole ratios of 1:1:400, 2:1:400 and 5:1:400. The reaction mixture proceeded under nitrogen atmosphere with vigorous stirring for 24 hours in a 50 mL round bottom flask at an ambient temperature of 35-40 °C. The dispersions were centrifuged thrice. Fresh ethanol was added each time followed by sonication to wash the nanoparticles before centrifugation. The siloxane functionalized nanoparticles were dried using a vacuum oven at 50 °C for 24 hours.

2.8. Spin Coating of nanoparticles on to glass slides

25 mm by 25 mm glass slides were thoroughly cleaned by sonicating in 70 % nitric acid for 10 minutes. They were rinsed with water and then with acetone and dried at 80 °C in a vacuum oven for 1 hour and thereafter, cooled in a vacuum desiccator. Thin films of ethanolic solutions of as-synthesized and functionalized nanoparticles were deposited on the glass slides using an Apex spinNXG-P2 spin coater at an ambient temperature of 24 °C. An initial acceleration of 500 rpm per second and a maximum speed of 6000 rpm for a total time of 60 seconds were maintained for all samples. Static dispense coating was used initially and followed up by dynamic dispense coating twice at 6000 rpm to achieve a uniform triple layer.

2.9. Characterization of nanoparticles

FTIR spectroscopy of nanoparticles was recorded by Thermo Nicolet Nexus 670 spectrometer. The groups attached to the nanoparticles were investigated by FTIR spectroscopy using the KBr disc method. PXRD measurement of the nanoparticles were performed in a θ-θ mode up to 80 degrees (2θ) by a Siemens D- 5000 X-ray diffractometer with Cu Kα radiation (λ = 0.154 nm) and a measurement temperature of 25 °C. The crystallite size "D" was obtained by the measurement of the broadening of diffraction lines and applying the Debye-Scherrer formula:

$$D=K\lambda/(\beta \cos\theta) \quad (1)$$

K =0.94 is the shape factor, λ is the X-ray wavelength of CuKα radiation (0.1542 nm), θ is the Bragg angle, and β is the experimental full-width at half-maximum (FWHM) of the respective diffraction peak (in units of radians). The hydrodynamic size of the nanoparticles was measured using (Nanosizer Nano ZS, Malvern) for dynamic light scattering. The nanoparticles were suspended in tetrahydrofuran and sonicated for twenty minutes at a temperature of 25 °C before the measurement. SEM was used to study the particle size and morphology of nanoparticles using an Olympus BX-51 scanning electron microscope at different magnifications. FESEM S4300 SEIN HITACHI at 10 kV was further used to produce higher resolution images to study the size and morphology of nanoparticles at different magnifications. Further image analysis was carried out using an ImageJ software. FESEM was operated concurrently with EDX which was used to investigate the elemental composition of nanoparticles. Water to air contact angles were measured following the procedures outlined in ASTM C813-9035 [25]. Apex ACAM-D1 which uses the sessile drop technique was used for the measurement at a temperature of 24 °C. An automatic droplet dispenser syringe was used to release a drop of permanganate distilled water onto the glass slide with care to avoid retraction. Contact angles were measured at left and right positions and averaged. For large variations in contact angles at the left and right positions, it was repeated either at a more levelled position or on a re-coated slide.

3. Results and discussion

3.1. Percent mass Yield

The mass of the calcined nanoparticles was obtained and measurement performed in triplicates with each measurement taken after a fresh reaction. Results of the mass of nanoparticles obtained as shown in Table 1 reveals that the mass of nanoparticles generally increased with increase in reaction volume. The reduction in percent mass yield as reaction volume increased signifies an increase in the probability of losing more nanoparticles at the washing stage with increasing reaction volume.

Table 1

Percentage mass yield of CeO_2 and SnO_2 nanoparticles

	Precursor (mL)	Mass (mg)	Expected mass (mg)	Percent Yield (%)
SnO_2	100	9.33±0.98	15.07	61.91
	200	17.25±1.25	30.14	57.23
	400	31.38±2.18	60.28	52.06
CeO_2	100	11.13±1.21	17.21	64.67
	200	21.90±1.68	34.42	63.63
	400	39.81± 2.37	68.85	60.46
ZrO_2	100	10.72±2.32	12.32	87.01
	200	20.70± 3.51	24.64	84.01
	400	38.44± 4.24	49.29	77.99

3.2 Fourier transform infra-red (FTIR)

As-synthesized ZrO_2 nanoparticles exhibited a broad frequency band at about 3481 cm^{-1} due to O-H stretching from residual alcohols, water and OH adsorbed onto the surface of ZrO_2 nanoparticles (Fig.1c). The bands at 2850

cm^{-1}, 1620 cm^{-1} and 1479 cm^{-1} can be attributed to C-H stretching and bending vibrations for CH_2 and CH_3 groups, respectively. The weak and intense bands at 1275 cm^{-1} and 1162 cm^{-1} are most likely due to the stretching vibrations of C-O. The band at 725 cm^{-1} can be attributed to Zr-O-Zr asymmetric stretching while the band at 512 cm^{-1} is due to Zr-O stretching which is very close to values reported by Tharani [26].

For the siloxane functionalized ZrO_2 nanoparticles (Fig.1d), the frequency band at 3484 cm^{-1} is related to O-H stretching from residual alcohols, water and OH adsorbed onto the surface of ZrO_2 nanoparticles. The band at 2982 cm^{-1} can be attributed to C-H stretching. The intense band at 1632 cm^{-1} is related to C=C stretching. Intense absorptions recorded at 1458 cm^{-1} and 1367 cm^{-1} are most likely due to the presence of CH_2 and CH_3 groups. The bands at 1221-1134 cm^{-1} can be attributed to C-F2. The peaks at 885 cm^{-1}, 805 cm^{-1}, 770 cm^{-1} and 710 cm^{-1} can be attributed to C-F3 bonds. The band at 503 cm^{-1} can be attributed to Zr-O bonds.

For as-synthesized CeO_2 nanoparticles (Fig.1e), the band at about 3368 cm^{-1} is due to O-H stretching from residual alcohols, water and OH adsorbed onto the surface of CeO_2 nanoparticles. The band at 2921 cm^{-1} is due to C-H stretching. The intense band at 1627 cm^{-1} can be attributed to C=C stretching vibration. The two absorptions recorded at 1385 cm^{-1} and 1320 cm^{-1} are most likely due to the presence of CH_2 and CH_3 groups. The band at 1079 cm^{-1} is due to the stretching vibrations of C-O. The band at 575 cm^{-1} can be attributed to Ce-O stretching. Ce–O stretching bands at 562 cm^{-1}, 459 cm^{-1} and at 451 cm^{-1} was reported by Yadav et al. [27], Maqbool et al. [16] and Arumugam et al. [14], respectively. The presence of groups such as reducing sugars, flavonoids and alkaloids were confirmed.

Siloxane functionalized CeO_2 nanoparticles (Fig.1f) showed a band at about 3399 cm^{-1} which is due to O-H stretching from residual alcohols, water and OH. The band at 2984 cm^{-1} can be attributed to C-H stretching. The intense band at 1630 cm^{-1} can be attributed to C=C stretching vibration. Intense absorptions recorded at 1472 cm^{-1} and 1325 cm^{-1} are most likely due to the presence of CH_2 and CH_3 groups. The frequency bands at 1243 cm^{-1}, 1212 cm^{-1} and 1106 cm^{-1} can be attributed to C-F2. The band at 1040 cm^{-1} can be attributed to Si-O-Si and peak at 964 cm^{-1} can be assigned to Si-O-C. The peaks at 894 cm^{-1}, 815 cm^{-1}, 744 cm^{-1} and 629-564 cm^{-1} can be related to C-F3 bonds. However, it seems that the C-F3 absorption band in 629-564 cm^{-1} may overlap the Ce-O band (575 cm^{-1}), which occurs in the same region.

As-synthesized SnO_2 nanoparticles exhibited a broad frequency band at about 3411 cm^{-1} due to O-H stretching from residual alcohols, water and OH adsorbed onto the surface of SnO_2 nanoparticles (Fig.1g). The bands at 2923 cm^{-1} and 2852 cm^{-1} are due to C-H stretching. The band at 1739 cm^{-1} is due to C–C stretching. The intense band at 1629 cm^{-1} can be attributed to C=C stretching vibration. The two absorptions recorded at 1457 cm^{-1} and 1379 cm^{-1} are most likely due to the presence of CH_2 and CH_3 groups. The weak and intense frequency bands at 1261 cm^{-1} and 1062 cm^{-1} are most likely due to the stretching vibrations of C-O. Peaks were observed at 568 cm^{-1} and 1079 cm^{-1} correspond to O-Sn-O bridge of SnO_2. This is in close agreement with previous studies conducted by Sudhaparimala et al. [28] and de Monredon et al. [29].

For the siloxane functionalized SnO_2 nanoparticles (Fig.1h), the frequency band at 3414 cm^{-1} is related to O-H stretching from residual alcohols, water and OH adsorbed onto the surface of SnO_2 nanoparticles. The band at 2979 cm^{-1} can be attributed to C-H stretching. The intense band at 1614 cm^{-1} is related to C=C stretching. Intense absorptions recorded at 1451 cm^{-1}, 1391 cm^{-1} and 1365 cm^{-1} are most likely due to the presence of CH_2 and CH_3 groups. The frequency bands at 1215-1122 cm^{-1} can be attributed to C-F2. The peaks at 878 cm^{-1}, 809 cm^{-1}, 780 cm^{-1} and 707 cm^{-1} can be related to C-F3 bonds. The band at 566 cm^{-1} can be attributed to O-Sn-O.

3.3 Powder X-ray Diffraction (PXRD)

Powder X-ray diffraction (PXRD) was performed to assess the crystalline nature, purity and crystallite size of the nanoparticles. PXRD was done before and after calcination. For as-synthesized ZrO_2 nanoparticles, the powder x-ray diffraction pattern (Fig.2a) showed a broad peak at 2θ of 10.39° corresponding to a crystallite size of 13.18 nm. For the calcined ZrO_2 nanoparticles (Fig.2b), peaks were sharp, indicating the crystalline nature of the nanoparticles. The peaks were located at 2θ of 30.29°, 35.11°, 50.47°, 60.00° corresponding to the crystallographic planes (111), (200), (220) and (311) respectively for monoclinic ZrO_2. All diffraction lines match closely with that of the standard data for monoclinic ZrO_2 (JCPDS Card number 37-1484) as shown by Shinde et al. [30]. A crystallite size of 4.24 nm was calculated using the Debye-Scherrer equation.

For as-synthesized CeO_2 nanoparticles (Fig.2b), a broad peak was at 22.69° corresponding to a crystallite size of 3.02 nm, highlighting their amorphous nature. Sharp peaks were observed for the calcined nanoparticles (Fig.2b), indicating their crystalline nature. Peaks corresponding to the fluorite structured CeO_2 crystal were observed at 2θ of 29.38°, 32.89°, 47.35°, 55.99°, 57.44° and 64.7° corresponding to the (111), (200), (220), (311), (222) and (400) planes, respectively. Prominent diffraction lines match closely with that of the standard data for fluorite cubic CeO_2 (JCPDS card number 00-0394). Crystallite size of 9.38 was obtained using the Debye-Scherrer equation.

For as-synthesized SnO_2 nanoparticles, the powder x-ray diffraction pattern (Fig.2c) showed a broad peak at 2θ of 10.27° corresponding to a crystallite size of 11.11 nm. For the calcined SnO_2 nanoparticles (Fig.2d), peaks were sharp, indicating the crystalline nature of the nanoparticles. The peaks were located at 2θ of 10.65°,

26.63°, 33.88°, 51.82° and 54.49° with 26.63°, 33.88°, 51.82° and 54.49° corresponding to the crystallographic planes (110), (101), (211) and (220) respectively, for tetragonal SnO_2. All diffraction lines match closely with that of the standard data for tetragonal SnO_2 (JCPDS card number 41-1445) shown in studies by Tan et al. [31] and Akhir et al. [32]. A crystallite size of 4.24 nm was calculated using the Debye-Scherrer equation.

An increase in the peak intensity values was observed with respect to calcination at 600 °C. This indicates an increase in the crystallinity of the nanoparticles. Higher crystallinity translates to improved properties such as stability and packing density.

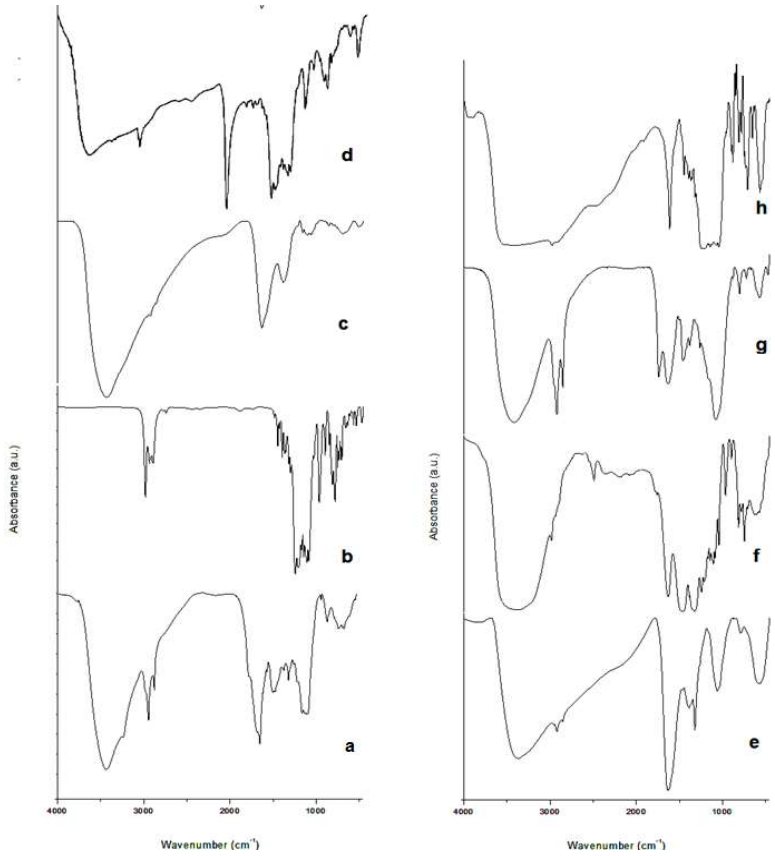

Fig.1. *FTIR spectra of (a)* A. indica *aqueous leaf extract, (b) FAS8261, (c) as-synthesized ZrO_2 nanoparticles, (d) functionalized ZrO_2 nanoparticles, (e) as-synthesized CeO_2 nanoparticles, (f) functionalized CeO_2 nanoparticles, (g) as-synthesized SnO_2 nanoparticles and (h) functionalized SnO_2 nanoparticles.*

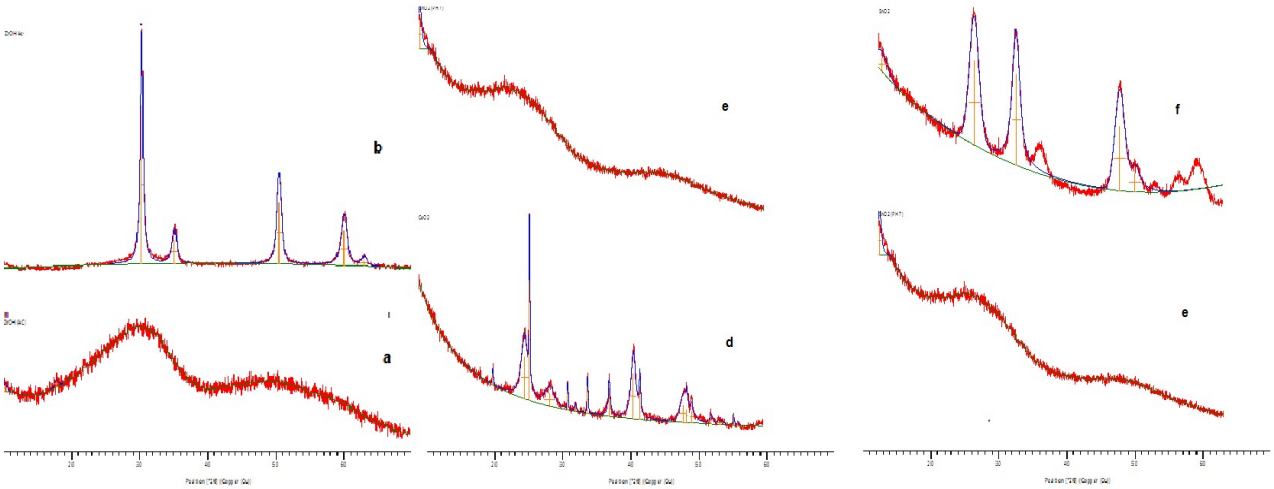

Fig.2. *XRD pattern of (a) as-synthesized ZrO_2 nanoparticles, (b) calcined ZrO_2 nanoparticles, (c) as-synthesized CeO_2 nanoparticles, (d) calcined CeO_2 nanoparticles, (e) as-synthesized SnO_2 nanoparticles (f) calcined SnO_2 nanoparticles*

3.4 Scanning electron microscopy (SEM)

SEM analysis was carried out to assess the morphology of the calcined bio-synthesized nanoparticles. The SEM image of the nanoparticles showed an onset of agglomeration. A spherical morphology was observed for the ZrO_2 nanoparticles (Fig.3a). Irregular morphologies were observed for CeO_2 (Fig.3b) and SnO_2 (Fig.3c) nanoparticles, with both having varying sizes of agglomerates.

3.5 Field emission scanning electron microscopy (FESEM)

FESEM provided further insight into the morphology and size details of the synthesized nanoparticles. The high-resolution study of the nanoparticles was carried out at different magnifications. Fig.4a showed spherical ZrO_2 nanoparticles having particle size of 10 nm with sparse lumps of agglomerates.

Fig.4b showed high density CeO_2 nanoparticles with scale-like arrangement, angular shapes and irregular morphology with predominant particles size of 12 nm. A bed of tiny SnO_2 nanoparticles having particle size of 6 nm with sparse lumps of agglomerates with sizes of up to 2 µm was observed in Fig.4c.

3.6 Energy dispersive X-ray spectroscopy (EDX)

The EDX spectrum of calcined nanoparticles confirmed the presence of elemental zirconium, cerium and tin at 64.0 %, 25.5 % and 53.7 % by weight respectively. The strong carbon signal observed for both nanoparticles is most likely as a result of organic groups from the plants that are adsorbed onto the surface of the nanoparticles. We can deduce that the adsorption of phytochemicals is in the order: $ZrO_2 < SnO_2 < CeO_2$. It is noteworthy that the nitrogen and chlorine in the precursors for CeO_2 and SnO_2 nanoparticles respectively were absent in the nanoparticles.

3.7 Contact angle measurement

To assess the wettability of glass substrate coated with as-synthesized and siloxane functionalized nanoparticles, contact angle measurements were performed using the static sessile drop method (Fig.5). The contact angle of bare glass was measured as 35.91° while 79.59° was obtained for the siloxane coated surface. Contact angles of 98.47°, 105.22°, 151.25° and 156.37° were obtained for glass slides coated with as-synthesized ZrO_2 nanoparticles and siloxane (FAS) functionalized nanoparticles with ZrO_2:FAS ratios of 5:1, 2:1 and 1:1, respectively.

Contact angles of 54.58°, 70.84°, 96.75° and 99.25° were obtained for glass slides coated with as-synthesized CeO_2 nanoparticles and siloxane (FAS) functionalized nanoparticles with CeO_2:FAS ratios of 5:1, 2:1 and 1:1, respectively. Contact angles of 96.17°, 107.62°, 112.65° and 119.44° were obtained for glass slides coated with as-synthesized SnO_2 nanoparticles and siloxane (FAS) functionalized nanoparticles with SnO_2:FAS ratios of 5:1, 2:1 and 1:1, respectively.

From Fig.7, we deduce that the non-wettable properties improved as available siloxane groups increased. Superhydrophobic surfaces were produced with ZrO_2 at nanoparticle to siloxane (NP: FAS) of 2:1 and 1:1. At NP: FAS 1:1, SnO_2 nanoparticles produced a highly non-wettable surface in contrast to non-wettable surfaces produced with CeO_2 nanoparticles.

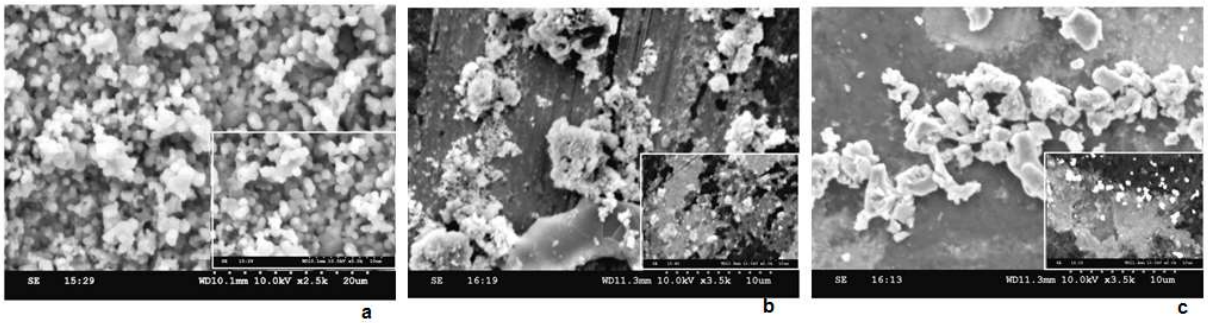

Fig.3. *SEM images of (a) ZrO_2 (b) CeO_2 (c) SnO_2 nanoparticles*

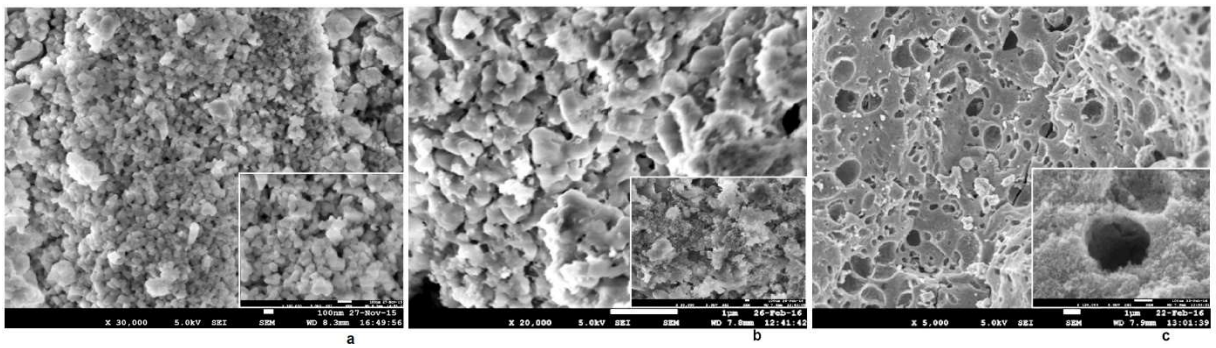

Fig.4. *FESEM images of (a) ZrO_2 (b) CeO_2 (c) SnO_2 nanoparticles*

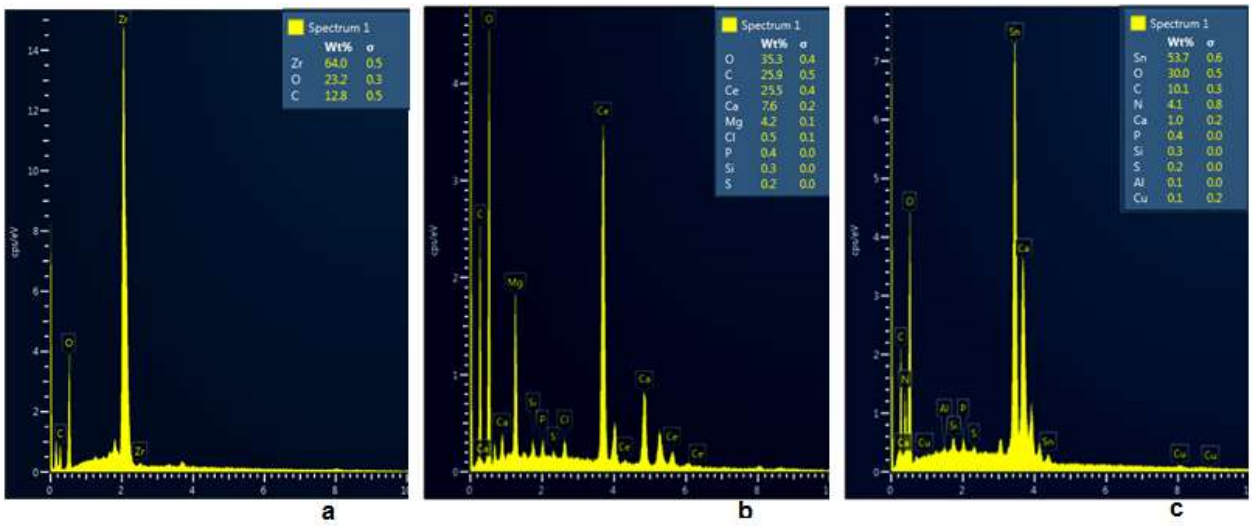

Fig.5. *EDX spectrum for (a) ZrO_2 (b) CeO_2 nanoparticles and (c) SnO_2 nanoparticles*

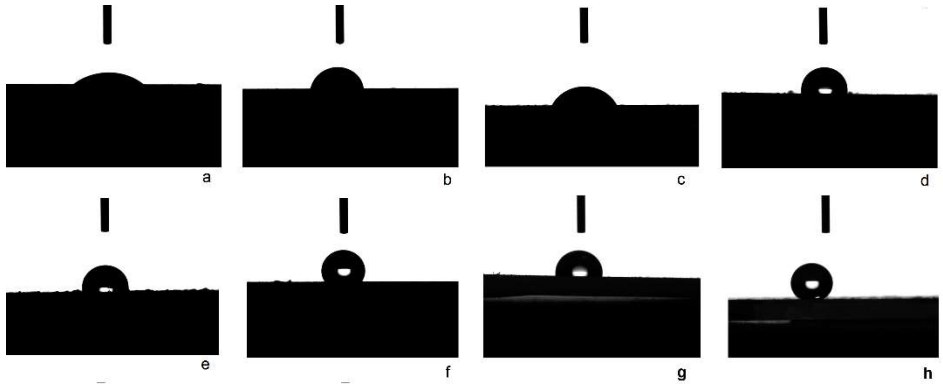

Fig.6. *Schematic diagrams showing a water droplet on: a) bare glass slide and glass slides coated with b) fluoroalkylsilane c) as-synthesized CeO_2 nanoparticles (d) functionalised CeO_2 nanoparticles (e) as-synthesized SnO_2 nanoparticles (f) functionalised SnO_2 nanoparticles (e) as-synthesized ZrO_2 nanoparticles (f) functionalised ZrO_2 nanoparticles*

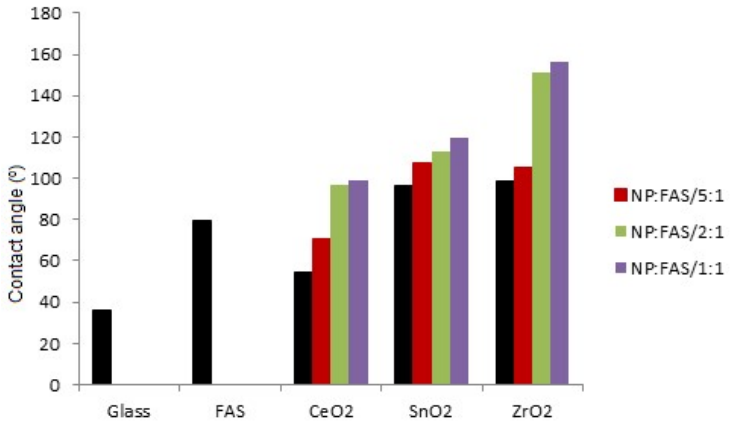

Fig.7. *Variation in contact angles for as-synthesized and functionalized: (a) ZrO_2, CeO_2 and SnO_2 nanoparticles.*

4. Conclusion

ZrO_2, CeO_2 and SnO_2 nanoparticles were successfully synthesized at ambient temperatures using the aqueous leaf extract of *A. indica* with percentage mass yields of over 60 % and particle sizes less than 20 nm for the metal oxide nanoparticles.

The suitability of three metal oxide nanoparticles synthesized via the phytochemical-mediated route for non-wetting applications was investigated. Interestingly, ZrO_2 nanoparticles showed the greatest potential in producing super-hydrophobic surfaces compared to CeO_2 and SnO_2 nanoparticles. From the EDX analysis, we deduced that phytochemicals were adsorbed strongest to the CeO_2 nanoparticles since it had the highest percentage carbon by weight compared to the ZrO_2 and SnO_2 nanoparticles. Strongly adsorbed phytochemicals could hinder siloxane molecules from binding to nanoparticles. That explains the low siloxane functionalization of CeO_2 nanoparticles. The more

defined spherical shape and relatively lesser degree of agglomeration observed for ZrO_2 nanoparticles would be responsible for the high degree of siloxane functionalization.

Water repellence generally improved with increasing siloxane concentration for the nanoparticles with maximum nanoparticle to fluoroalkylsilane mole ratio of 1 to 1 producing non-wettable, strongly non-wettable and super-hydrophobic surfaces for CeO_2, SnO_2 and ZrO_2 nanoparticles, respectively. A further publication will incorporate ultra-sonication, acid treatment or etching of as-synthesized nanoparticles as additional processing techniques to remove strongly adsorbed phytochemicals without further agglomeration so as to improve the water repellence properties of the siloxane functionalized phyto-synthesized nanoparticles in order to enhance their suitability towards the production of super-hydrophobic coatings for potential biomedical, agricultural and industrial coating applications.

Conflicts of interest

The authors declare that they have no conflict of interest.

Authorship statement

O.S. Bankole-Ojo: Conceptualization, Methodology, software, original draft preparation. F.O. Oyedeji: Supervision, reviewing and editing. N. Ramanuj: Data curation, supervision.

Acknowledgement

The present research work was funded by CSIR-TWAS Postgraduate fellowship. The authors would like to thank the Director, CSIR-IICT and extend their appreciation to the entire staff and students of Polymers and Functional Materials division, CSIR-IICT, India for their support. Appreciation goes to the authorities of the University of Ibadan, Nigeria for permission granted to execute the research.

References

[1] L. Yin, Y. Wang, G. Pang, Y. Koltypin, A. Gedanken, Journal of Colloid and Interface Science 246 (2002) 78-84.
[2] R. Chakravarty, S. Chakraborty, R. Shukla, J. Bahadur, R. Ram, S. Mazumder, H.D. Sarma, A.K. Tyagi, A. Dash, Dalton Transactions 45 (2016) 13361-13372.
[3] G. Shen, Q. Wang, Z. Wang, Y. Chen, Materials Letters 65 (2011) 1211-1214.
[4] A. Mirzaei, G. Neri, Sensors and Actuators B: Chemical 237 (2016) 749-775.
[5] C.J. Shih, Y.J. Chen, M.H Hon, Materials Chemistry and Physics 121 (2010) 99-102.
[6] N.S. Ferreira, R.S. Angélica, V.B. Marques, C.C.O. De Lima, M.S. Silva., Materials Letters 165 (2016) 139-142.
[7] V.V. Makarov, A.J. Love, O.V. Sinitsyna, S.S. Makarova, I.V. Yaminsky, M.E. Taliansky, N.O. Kalinina, Acta Naturae 6 (2014) 35-44.
[8] K.N. Thakkar, S.S. Mhatre, R.Y. Parikh, Nanomedicine: Nanotechnology, Biology and Medicine 6 (2010) 257-262.
[9] S. Gowri, R.R. Gandhi, M. Sundrarajan, Journal of Materials Science & Technology 30 (2014) 782-790.
[10] P. Nimare, P., A.A. Koser, International Research Journal of Engineering and Technology 3 (2016) 1910-1912.
[11] R.D. Abdul Jalill, M.M.H.M. Jawad, A.N. Abd, Journal of Genetic and Environmental Resources Conservation 5 (2017) 6-23.
[12] S.K. Kannan, M. Sundrarajan, International journal of nanoscience 13 (2014) 1450018.
[13] G.S. Priya, A. Kanneganti, K.A. Kumar, K.V. Rao, S. Bykkam, International Journal of Scientific and Research Publications 4 (2014) 199-224.
[14] A. Arumugam, C. Karthikeyan, A.S.H. Hameed, K. Gopinath, S. Gowri, V. Karthika, Materials Science and Engineering: C 49 (2015) 408-415.
[15] N. Thovhogi, A. Diallo, A. Gurib-Fakim, M. Maaza, Journal of Alloys and Compounds 647 (2015) 392-396.
[16] Q. Maqbool, M. Nazar, S. Naz, T. Hussain, N. Jabeen, R. Kausar, S. Anwaar, F. Abbas, T. Jan, International journal of nanomedicine 11 (2016) 5015.
[17] N. Srivastava, M. Mukhopadhyay, Industrial & Engineering Chemistry Research 53 (2014) 13971-13979.
[18] P. Kamaraj, R. Vennila, M. Arthanareeswari, S. Devikala, Pharmacy and Pharmaceutical Science 3 (2014) 382-338.
[19] V.K. Vidhu, D. Philip, Spectrochimica Acta Part A: Molecular and Biomolecular Spectroscopy 134 (2015) 372-379.
[20] L. Fu, Y. Zheng, Q. Ren, A. Wang, B. Deng, Journal of Ovonic Research 11 (2015) 21-26.
[21] S.E. Atawodi, J.C. Atawodi, Phytochemistry Reviews 8 (2009) 601-620.
[22] R. Campos, A.J. Guenthner, T.S. Haddad, J.M. Mabry, Langmuir 27(16) (2011) 10206-10215.
[23] R. Madhusudhana, M.A. Sangamesha, R. Gopal Krishne, L. Krishnamurthy, G.L. Shekar, International Journal of Advanced Research 2 (2014) 433-436.
[24] S. Pazokifard, S.M. Mirabedini, M. Esfandeh, Advanced Powder Technology (2012) 23, 428-436.
[25] ASTM C813-90, Standard Test Method for Hydrophobic Contamination on Glass by Contact Angle Measurement, ASTM International. (2014)
[26] S.S.N. Tharani, International Journal of Engineering and Applied Sciences 3 (2016) 23-25.
[27] L.R. Yadav, K. Manjunath, B. Archana, The European Physical Journal Plus 131 (2016) 154.
[28] S. Sudhaparimala, A. Gnanamani, A.B. Mandal, American Journal of Nanoscience and Nanotechnology 2 (2014) 75-83.
[29] S. de Monredon, A. Cellot, F. Ribot, C. Sanchez, L. Armelao, L. Gueneau, L. Delattre, Journal of Materials Chemistry 12 (2002) 2396-2400.
[30] H.M. Shinde, T.T. Bhosale, N.L. Gavade, S.B. Babar, R.J. Kamble, B.S. Shirke, K.M. Garadkar, Journal of Materials Science: Materials in Electronics 29 (2018) 14055-14064.
[31] L. Tan, L. Wang, Y. Wang, Journal of Nanomaterials (2011) 23.
[32] M.A. Akhir, K. Mohamed, H.L. Lee, S.A. Rezan, Procedia Chemistry 19 (2016) 993-998.